Static Aerodynamics of Missile Configurations for Mach 0 to 3

F. G. Moore*
Naval Surface Weapons Center, White Oak Laboratory, Silver Spring, Md.

Several theoretical and empirical procedures are combined to form a useful design tool for computing static aerodynamics on gun-launched guided projectiles and missiles. The Mach number and angle-of-attack range over which the method is applicable are $0 \leq M_\infty \leq 3$ and $0 \leq \alpha \leq 15°$, respectively. Body and wing geometries can be quite general in that pointed or blunt nose bodies and sharp or blunt leading-edge wings can be assumed. Computed results for several configurations compare well with experimental and other analytical results. The computer program is cost effective as it only costs about $5 per Mach number to compute the lift, drag, and pitching moment of a typical wing-body shape on the CDC 6700 Computer.

Nomenclature

AR = aspect ratio
b = wing span (does not include body radius)
c = chord length at any point along span
C_A = axial force coefficient = C_{D0}
C_{AB} = trailing-edge separation drag coefficient
C_{D0} = zero lift drag coefficient
C_M = pitching moment coefficient measured about nose tip (positive nose up)
C_{M_α} = pitching moment coefficient derivative ($dC_M/d\alpha$)
C_N = normal force coefficient
C_{N_α} = normal force coefficient derivative ($dC_N/d\alpha$)
C_P = pressure coefficient
C_{P_B} = base pressure coefficient
C_{P0} = stagnation pressure coefficient
c_{r1} = chord length at root of the leading-edge portion of a modified double wedge airfoil section
c_{r2} = chord length at root of the trailing-edge portion of a modified double wedge airfoil section
d = body diameter
$K_{B(w)}$ = ratio of lift of body in presence of wing to that of the wing alone
$K_{w(B)}$ = ratio of lift of wing in presence of body to that of wing alone
$k_{B(w)}$ = ratio of lift on body in presence of wing, due to a wing deflection, δ, to that of wing alone
k_i = $k_i = \tan \Lambda_i$
$k_{w(B)}$ = ratio of lift of wing in presence of body, due to a wing deflection, δ, to that of wing alone
M = Mach number
r = radius of body (variable)
r_{LE} = radius of wing leading edge in a plane normal to leading edge
r_{TE} = radius of wing trailing edge in a plane normal to trailing edge
S_{ref} = reference area (maximum body cross-sectional area unless wing alone is considered in which case the wing planform area is used)
S_w = wing planform area
s = wing semispan plus body radius at wing root chord
t = wing thickness (variable)
u,v,w = perturbation velocities in the x, y, z directions, respectively
V = total velocity, $V^2 = (U_\infty + u)^2 + v^2 + w^2$
x,y,z = rectangular coordinate system with x at nose tip, y out right wing, and z positive up. If no body is present, x begins at wing root chord.
α = angle of attack
β = $(M_\infty^2 - 1)^{1/2}$
γ = ratio of specific heats ($\gamma = 1.4$ for air)
δ = angle between a tangent to the local body or wing surface and freestream direction
ϵ_1 = angle on blunt leading edge where Newtonian theory stops and perturbation theory begins (match point)
θ = cylindrical coordinate measured with $\theta = 0$ in leeward plane
Λ_i = sweepback angle of a wing generator ($i = 1, 2, 3, 4$) with $i = 1$ the wing leading edge and $i = 4$ the wing trailing edge
λ = ratio of tip chord to root chord (c_t/c_r)
μ = Mach angle, $\mu = \sin^{-1}(1/M_\infty)$
ϕ = velocity potential
χ = wedge half angle (measured parallel to freestream) of wing airfoil section

Subscripts

cp = center of pressure
fb = force break Mach number
r = root chord
t = tip chord
I = wing for which slender body values of interference lift are known
II = wing with sweep for which representative values of interference lift are desired
∞ = freestream conditions

Submitted June 14, 1974; presented as Paper 74-538 at the AIAA 7th Fluid and Plasma Dynamics Conference, Palo Alto, California, June 17-19, 1974; revision received January 17, 1975. Research sponsored by Naval Sea Systems Command under SEATASK 35A-501/090-1/UF 32-323-505.

Index categories: Aircraft Aerodynamics (including Component Aerodynamics); Subsonic and Transonic Flow; Supersonic and Hypersonic Flow.

*Research Aerospace Engineer, Advanced Weapons Department. Member AIAA.

I. Introduction

QUITE often the aerodynamicist, when he works with or near a design group, is faced with the task of estimating such important design parameters as range, static margin, maneuverability, and other design properties of a given configuration. Once the design engineer obtains the data he is seeking, the next question the aerodynamicist must answer is, "How can I improve the configuration so its

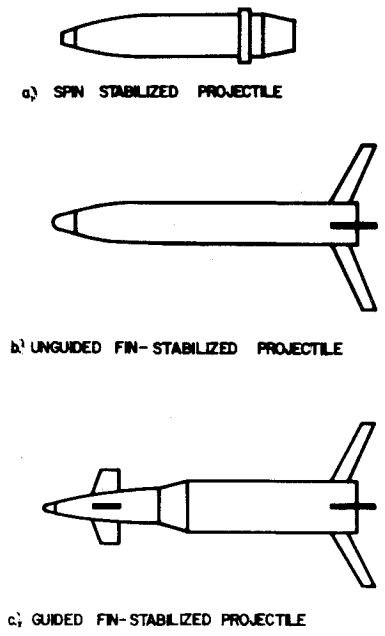

Fig. 1 Basic configurations (illustration only).

aerodynamic properties are better?" Ultimately, an iteration cycle will probably be made in which several different configurations will be considered before the two or three most optimum candidates are chosen for further study. The important point to be made here is that for each of the aforementioned configurations, static aerodynamics (lift, drag, and pitching moment) must be estimated before questions concerning such things as range and maneuverability can be answered.

To obtain this set of aerodynamic coefficients, the engineer can go one of three directions: he can conduct a wind tunnel test which will be costly and time consuming and probably produce results which are more accurate than warranted for preliminary and intermediate design; he can perform hand calculations using handbook techniques[1] and applicable experimental data but not have a good accuracy estimate of the results; or he can develop a computer program based on analytical techniques which is efficient and produces accuracies on the order of $\pm 10\%$. The latter alternative, although being more costly and time-consuming initially, is the best approach for long-term use and is the procedure which will be addressed in this paper.

To be of practical use to the Navy, the theory must compute static aerodynamics for the Mach number and angle-of-attack range of most projectiles and missiles, that is $0 \leq M_\infty \leq 3$ and $0 \leq \alpha \leq 15°$, respectively. Also, quite general body and wing geometries must be considered. This arises from the fact that projectile noses may be pointed, truncated, or spherically blunt. Another contributing factor to the complex geometries is the high setback forces at launch which means the wings and canards must be quite thick to survive the initial g loads. Moreover, there may be two ogives on the nose (in the case of a fuze or blunt seeker) and a boattail present for drag reduction purposes. Figure 1 illustrates the general type of projectile geometries that are encountered. Designing a computer program to handle such complex geometries means that most missile configurations can also be considered.

Several works existed previously which could fulfill portions of the present goal of a general aerodynamic prediction program, but none of which was satisfactory in its entirety. The most notable of these is that due to Woodward.[2] Woodward uses perturbation theory to compute the pressure distrubition on wing-body combinations in subsonic and supersonic flow. However, the bodies must be pointed and the wing leading edge sharp. Also, he does not calculate the base and skin-friction drag or the nonlinear angle of attack effects. Moreover, no consideration is given to transonic flow.

COMPONENT \ MACH NUMBER REGION	SUBSONIC	TRANSONIC	SUPERSONIC
NOSE WAVE DRAG	——	Wu and AOYOMA PLUS EMPIRICAL	2nd ORDER VAN DYKE PLUS MODIFIED NEWTONIAN
BOATTAIL WAVE DRAG	——	Wu and AOYOMA	2nd ORDER VAN DYKE
SKIN FRICTION DRAG	VAN DRIEST II		
BASE DRAG	EMPIRICAL		
INVISCID LIFT and PITCHING MOMENT	EMPIRICAL	Wu and AOYOMA PLUS EMPIRICAL	TSIEN 1st ORDER CROSSFLOW
VISCOUS LIFT and PITCHING MOMENT	ALLEN and PERKINS CROSSFLOW		

Fig. 2 Methods used to compute body-alone aerodynamics.

Another method available for calculating aerodynamics on wing-body configurations is that of Saffell et al.[3] This procedure computes static aerodynamics on low aspect-ratio missile configurations. Its applicability to general aspect-ratio configurations is thus questionable, particularly at small α. Furthermore, drag was calculated by handbook techniques[1] and is also quite inaccurate at small α. The last method of practical use in projectile work is the all-empirical GE "Spinner" program.[4] However, its applicability is for spin-stabilized projectiles only. Thus, guided projectiles (or missiles) cannot be considered.

It is apparent then, from the preceding discussion, that there is a definite need for an analytical method to compute static aerodynamics which can take into account body nose and wing leading-edge bluntness, angle of attack, and still cover subsonic through supersonic flow. The theory should be accurate enough to replace preliminary and intermediate wind-tunnel testing yet computationally fast enough so it can be used as an efficient design tool.

II. Analysis

Body-Alone Methods

The body-alone work has been presented previously[5] and as such will only be highlighted for continuity purposes in this paper. For further details, see either Ref. 5 or 6.

A summary of the various analytical and empirical procedures which have been combined to compute lift, drag, and pitching moment for complex body geometries and at $0 \leq \alpha \leq 15°$ and $0 \leq M_\infty \leq 3$ are shown in Fig. 2. Most of the methods are standard in the literature with the exception of the combined Newtonian-perturbation theory used to calculate nose wave drag. Since this procedure is new, it will be briefly outlined.

For pointed nose bodies where the local body slope is less than the freestream Mach lines, Van Dyke's perturbation theory is sufficient to calculate the entire pressure distribution. If the nose is blunt, the perturbation theory is not applicable at the nose tip so it is combined with modified Newtonian theory.

The modified Newtonian pressure coefficient is

$$C_P = C_{p0} \sin^2 \delta \tag{1}$$

where the stagnation pressure coefficient behind a normal shock is

$$C_{p0} = \frac{2}{\gamma M_\infty^2} \left[\left[\frac{(\gamma+1)M_\infty^2}{2} \right]^{\gamma/(\gamma-1)} \times \left[\frac{\gamma+1}{2\gamma M_\infty^2 - (\gamma-1)} \right]^{1/(\gamma-1)} - 1 \right] \tag{2}$$

and where δ is the slope of the surface relative to the freestream. For a spherical nose this is

$$\delta = \sin^{-1}[\sin\beta' \cos\alpha - \cos\beta' \cos\theta \sin\alpha] \quad (3)$$

where $\tan\beta' = dr/dx$.

Assuming that the pressure coefficient over that portion of the body where the local slope is small can be calculated by perturbation theory, the only question that now remains so far as the supersonic Mach number region is concerned is where does the modified Newtonian theory end on the surface and where does the perturbation theory begin. To determine this match point, recall that the slope of the body surface must be less than the Mach angle to apply perturbation theory, that is $\delta \leqslant \sin^{-1}(1/M_\infty)$. Thus, the upper limit of the perturbation theory is

$$\delta = \sin^{-1}(1/M_\infty) \quad (4)$$

Using this relation in Eq. (3) and assuming a spherical nose cap there is obtained for the coordinates of the point below which Newtonian theory must be applied

$$r_u = r_n/M_\infty [(M_\infty^2 - 1)^{1/2}\cos\alpha + \sin\alpha]$$

$$x_u = r_u \tan\alpha + r_n[1 - 1/(M_\infty \cos\alpha)] \quad (5)$$

It is important to note here that if $x > x_u$ Newtonian theory may still be applied but if $x < x_u$ perturbation theory cannot be applied.

The limiting angle of Eq. (4) corresponding to the coordinates of Eq. (5) is shown in Fig. 3 as the upper curve. Note that very large angles can be considered using the perturbation theory at the lower Mach numbers. However, as shown by Van Dyke[7] the loss in accuracy of perturbation theory increases rapidly as the angle δ is increased. Realistically, since at an angle of 25°-30° the error is still slight the maximum angle δ for which perturbation theory is applied should not exceed these values. Based on these accuracy considerations, the Newtonian theory should be applied for δ values outside the solid line boundary of Fig. 3 and perturbation theory within the boundary. Now the match point, which is defined as the point where the pressure coefficients of the Newtonian theory and the perturbation theory are equal, can be determined as the solution proceeds downstream. For body stations downstream of the match point, perturbation pressures are used in the force coefficient calculations whereas for x values along the surface less than that at the match point, Newtonian pressures must be used. This is indicated qualitatively in Fig. 4 where x_2 is the match point for second-order perturbation and Newtonian theory and x_1 the match point for first-order perturbation and Newtonian theory.

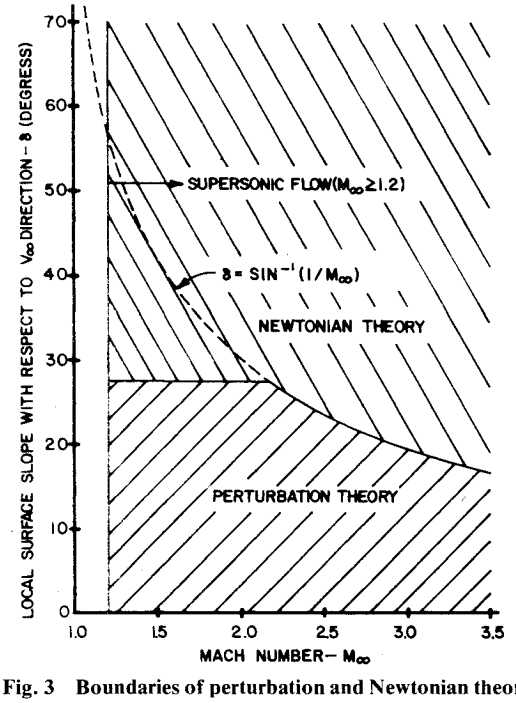

Fig. 3 Boundaries of perturbation and Newtonian theory.

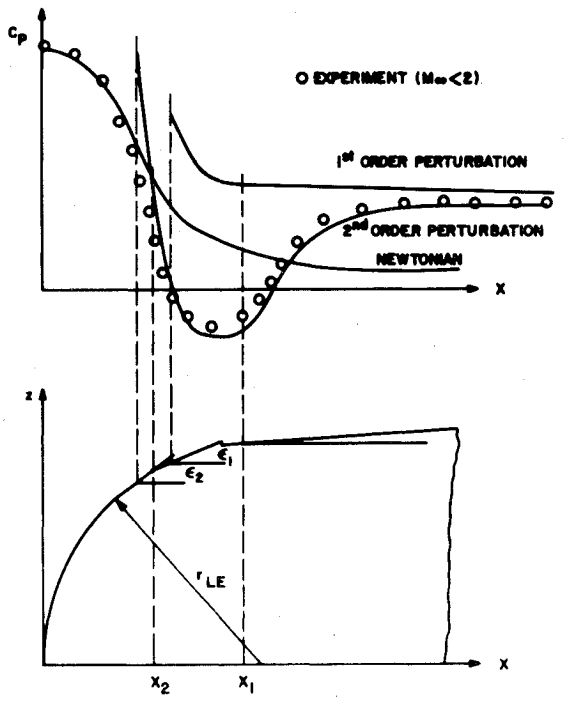

Fig. 4 Combined Newtonian and perturbation theory for a blunt leading edge.

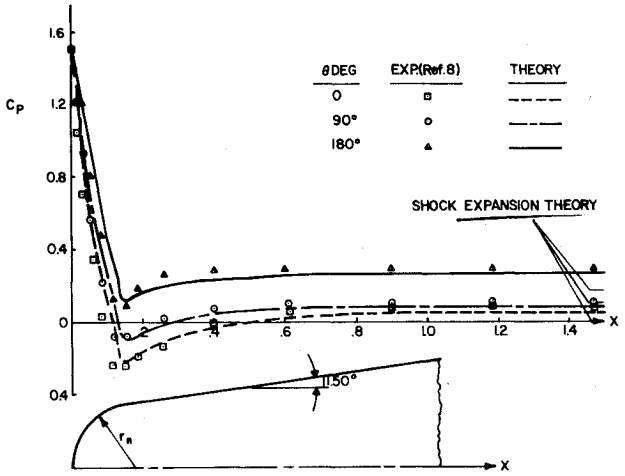

Fig. 5 Comparison of theory and experiment for blunted cone; $r_n/r_B = 0.35$, $M_\infty = 1.5$, and $\alpha = 8°$.

It is of interest to compare the pressure coefficients predicted by the combined perturbation Newtonian theory with experiment. Figure 5 presents a typical comparison at $M_\infty = 1.5$. These experimental data are taken from Ref. 10 which combined modified Newtonian theory with shock expansion theory to compute forces on blunted cones. The asymptotes of the pressure coefficient in each of the planes computed by the method of Ref. 10 are also indicated on the figures. As seen in the figure, the present theory predicts the aerodynamics much better than shock expansion theory at $M_\infty = 1.5$. For the very same blunted cone at $M_\infty = 2.96$ (not shown) the present method gave values for the pressure and force coefficients which were about the same as those of shock expansion theory. The reason for this is that the per-

turbation theory was derived assuming shock-free flow with entropy changes slight; hence the theory should be most accurate in the lower supersonic speed regime. On the other hand, shock expansion theory was derived assuming a shock present and so one would expect this method to be better than perturbation theory as M_∞ is increased. Apparently, the crossover point is around $M_\infty = 2.5$ to 3.0 so that for the major portion of the supersonic speed range of interest in the present analysis, perturbation theory is more accurate.

Another interesting point in Fig. 5 is the discontinuity in slope of the pressure coefficient curve which occurs at the match point. This is because in the expansion region on the spherical nose the perturbation pressure decreases much more rapidly than the Newtonian theory and, as a result, the overexpansion region, which occurs at low supersonic Mach numbers, is accounted for quite well. Note that the match point is different in each plane around the surface ($x \cong 0.11$ to 0.14).

Wing and Wing-Body Interference Methods

A summary of the various theories used for calculating static aerodynamics of the wing alone and for computing the wing-body interference lift is given in Fig. 6. Several of the methods are standard in the literature and could be applied directly with no modifications. For example, the wing lift was calculated by linear theory[11] in supersonic flow and by lifting surface theory[12] in subsonic flow. Knowing the lift coefficient at the lowest supersonic Mach number computed, $M_\infty = 1.2$, and at the highest subsonic Mach number, $M_\infty = M_{fb}$, one can then empirically define the lift in the transonic speed regime. The technique used is that described in DATCOM[1] and is a function of wing sweep, Mach number, aspect ratio, and wing-thickness ratio. Also the wing-tail interference lift was computed by standard line vortex theory[13] and the skin friction drag by the method of Van Driest.[14] Reference 15 gives a detailed discussion of these methods.

For the remaining static aerodynamics, that is wing-body interference lift, wave drag, trailing-edge separation drag, and body base pressure drag caused by the tail fins, existing methods had to be modified or empirical procedures developed for calculation purposes. These new methods will now be discussed individually.

Wing Wave Drag

It will be assumed a priori that the wing is symmetric about the x-y plane so that no camber is present. Furthermore, the wing will be assumed to be thin with either a modified double wedge (Fig. 7) or biconvex airfoil section. However, by assuming a modified double wedge only requires that straight lines exist between points A and B, B and C, and D and E (see Fig. 7). These straight lines could then be any percentage of the entire chord. For example, if BD were zero the airfoil would be a double wedge design or if both BD and DE were zero, the airfoil would be a wedge. Also, either the biconvex

COMPONENT \ MACH NUMBER REGION	SUBSONIC	TRANSONIC	SUPERSONIC
INVISCID LIFT AND PITCHING MOMENT	LIFTING SURFACE THEORY	EMPIRICAL	LINEAR THEORY
WING-BODY INTERFERENCE	SLENDER BODY THEORY AND EMPIRICAL		LINEAR THEORY, SLENDER BODY THEORY & EMPIRICAL
WING-TAIL INTERFERENCE	LINE VORTEX THEORY		
WAVE DRAG	—	EMPIRICAL	LINEAR THEORY + MODIFIED NEWTONIAN
SKIN FRICTION DRAG	VAN DRIEST		
TRAILING EDGE SEPARATION DRAG	EMPIRICAL		
BODY BASE PRESSURE DRAG CAUSED BY TAIL FINS	EMPIRICAL		

Fig. 6 Methods used to compute wing alone and interference aerodynamics.

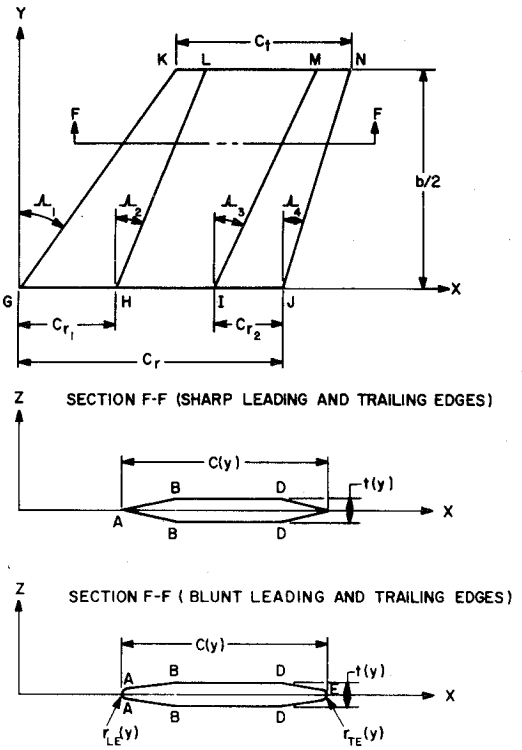

Fig. 7 Wing with modified double wedge airfoil section.

or modified double wedge design or if both BD and DE were zero, the airfoil would be a wedge. Also, either the biconvex or modified double wedge design may have blunt leading and trailing edges and the thickness to chord ratio may vary along the span. The wing generators GK, HL, IM, and JN are assumed straight.

Since the wing is thin, the linearized three-dimensional equation of motion governing the steady flowfield is[11]

$$\beta^2 \phi_{xx} - \phi_{yy} - \phi_{zz} = 0 \tag{6}$$

where subscripts indicate partial differentiation. Here, the velocity potential ϕ is related to the perturbation velocities by

$$\phi_x = u \tag{7a}$$

$$\phi_y = v \tag{7b}$$

$$\phi_z = w \tag{7c}$$

The boundary conditions required for the solution of the linear partial differential Eq. (1) are that the flow must be tangent to the surface

$$w(x,y) = \phi_z(x,y,0^-) = \phi_z(x,y,0^+) = (\partial F/\partial x)\,(x,y) \tag{8}$$

and that the perturbation velocities must vanish upstream of the most forward point of the wing. Referring to Fig. 7, this most forward point is at $x = 0^-$ so that the second boundary condition is

$$\phi_x(0^-,y,z) = \phi_y(0^-,y,z) = \phi_z(0^-,y,z) = 0 \tag{9}$$

The plus or minus superscript means the particular axis is approached from the positive or negative side, respectively. Because of the symmetry of the airfoil, Eq. (8) indicates that it makes no difference from which side one approaches the axis $z = 0$.

Equation (6) is valid only where the perturbation velocities are small. This means that in the neighborhood of a blunt leading or trailing edge, some other method must be applied.

Consider first a general three-dimensional wing with sharp leading and trailing edges.

The general solution to Eq. (6) along the airfoil surface ($z \cong 0$) is[16]

$$\phi(x,y,0) = -\frac{1}{\pi}\int\int_{\Sigma} \frac{w(x_1,y_1)\,dx_1 dy_1}{[(x-x_1)^2-\beta^2(y-y_1)^2]^{1/2}} \tag{10}$$

where Σ indicates the region of integration. The source strength $w(x_1,y_1)$ is related to the local slope of the airfoil surface through the boundary condition Eq. (8).

In previous works $w(x_1, y_1)$ was assumed constant or a function of x only (the slope of the airfoil surface was the same all along the span), so the integration of the above integral could be carried out in closed form for simple wing planforms.[16] In the present analysis, the slope of the wing is allowed to vary in the spanwise as well as the chordwise direction so the integration of Eq. (10) cannot, in general, be carried out in closed form. One approach would be to define the slope of the given surface and carry out the double integration by numerical quadrature. However, one must be aware of the singular nature of the double integral where $(x-x_1)^2 = \beta^2 (y-y_1)^2$ during the integration process. A simpler approximate method, in analogy to the tangent wedge or tangent cone theories, is to assume that on a small element of the wing surface, $w(x_1, y_1)$ is constant. Then, if the region of integration of Eq. (10), Σ ,is assumed to be over a small element of the wing, one may write

$$\phi(x,y,0) = -\frac{w(x,y)}{\pi}\int\int_{\Sigma} \frac{dx_1 dy_1}{[(x-x_1)^2-\beta^2(y-y_1)^2]^{1/2}} \tag{11}$$

Equation (11) is now in the form given in Ref. 16 for simple planform geometries and the integration can be carried out directly. Again it should be emphasized that $w(x,y)$ is the slope of the airfoil surface at a given point and may vary for each element of the wing.

This analysis applies to airfoils with sharp leading and trailing edges. If the airfoil leading or trailing edge is blunt, some other method must be applied in the vicinity of the blunted portion because the assumptions of perturbation theory are violated there. In analogy to the body-alone work discussed previously, modified Newtonian Theory will be applied to the blunt leading edges and an empirical afterbody separation pressure correction applied at the blunt trailing edges as will be discussed later.

If it is assumed the blunt leading edge of the wing is cylindrical in a direction perpendicular to the leading edge, then this circular shape appears as an ellipse in the streamwise direction for sweptback wings. Thus, for a given point on the airfoil leading edge with coordinates (x,y,z), it can be shown that the slope δ of Eq. (1) is

$$\delta(x,y,z) = \tan^{-1}[\tfrac{1}{3}\cos\Lambda_1 (r_{LE}(y) - x\cos\Lambda_1)] \tag{12}$$

Note that Eq. (12) assumes the leading-edge radius may vary along the span, that is $r_{LE} = r_{LE}(y)$. The pressure coefficient over the elliptical leading edge can now be calculated at each airfoil section by combining Eqs. (1, 2, 12, and 18).

In analogy to the body-alone work, the question again arises concerning the match point between the modified Newtonian Theory and first-order perturbation theory. In the body alone work, the second-order perturbation theory was started as far upstream on the spherical cap as possible while still getting reasonably accurate perturbation pressure coefficients. It was found that slopes of 25-30° were optimum. Although the results were unpublished, it was found in that work that if first-order instead of second-order perturbation theory were used, this angle must be reduced to about 15°. Also, it was found that second-order theory accounted very well for the over-expansion region around the spherical cap whereas the first-order theory did not. The important analogy to be drawn from this discussion is that for three-dimensional wings, a first-order (rather than a second-order) theory is combined with modified Newtonian theory to calculate wave drag when the leading edge is blunt. Thus, in analogy to bodies of revolution, one would intuitively expect the angle where perturbation theory begins to be around 15°. A discontinuity in pressure coefficients of Newtonian and perturbation theory is expected at the match point due to the failure of the first-order theory to account for the over-expansion region, as shown qualitatively in Fig. 4.

If the first-order pressure coefficients are computed at $\epsilon_1 = 15°$ (see Fig. 4), and the flow allowed to expand to the match point x_1, the drag coefficient of the blunt leading edge can be found as

$$C_{A_{LE}} = \frac{4R_{avg}bC_{p0}\cos^2\Lambda_1}{S_{ref}}\left[\sin\epsilon_u - \frac{\sin^3\epsilon_u}{3}\right] \tag{13}$$

where

$$R_{avg} = \frac{(r_{LE})_r + (r_{LE})_1}{2}$$

and ϵ_u is the angle corresponding to x_1. The drag of the section aft of the cylindrical leading edge can be found by numerical quadrature of the integral

$$C_D = \frac{8}{S_w}\int_0^{b/2}\int_{c(x_1)}^{c(y)} C_p(x,y)\,w(x,y)\,dx\,dy \tag{14}$$

where $C_p(x,y) = -2\phi_x(x,y,0)$ and ϕ_x is found from standard closed formed solutions of Eq. (11) at each point as discussed.

Wing Trailing-Edge Separation Drag

If the trailing edge is blunt or if its slope is large, the boundary layer will separate somewhere on the rear of the wing. This results in a high drag region similar to that on the base of a projectile, except here the separation is a two-dimensional as opposed to a three-dimensional phenomenon. The pressure on the rear of the wing will then be that of a two-dimensional rearward facing step. Chapman[17] presents experimental results for a blunt wing with no slope at the trailing edge. These results are presented in Fig. 8 as a function of Mach number. Note that the data for $M_\infty < 1.1$ has been extrapolated based on the general shape of the three-dimensional base pressure curve presented in Ref. 6. If $(r_{TE})_r$

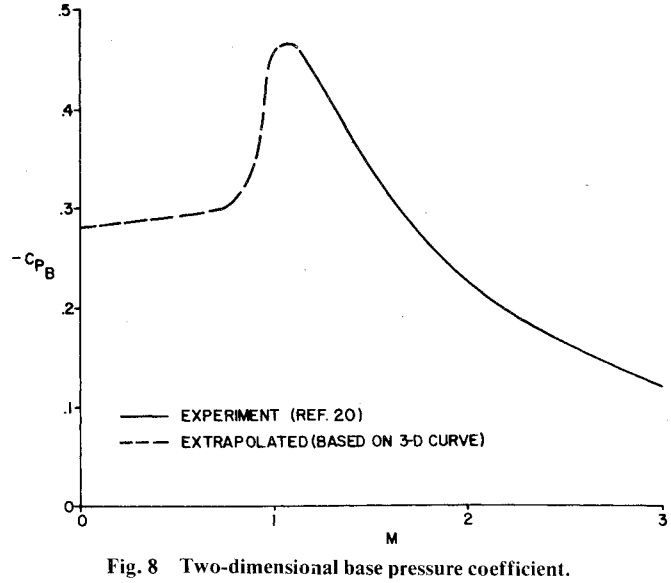

Fig. 8 Two-dimensional base pressure coefficient.

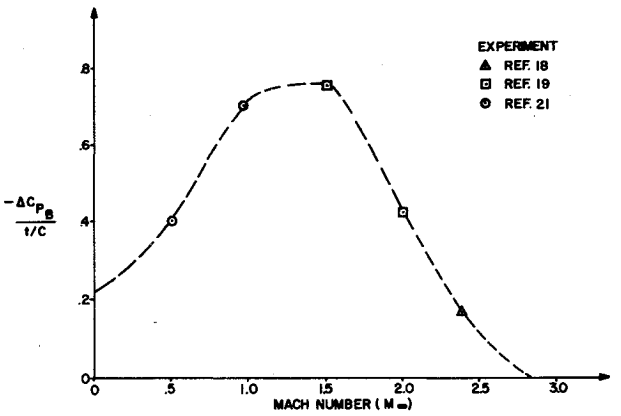

Fig. 9a Base pressure coefficient change with fins located flush with base.

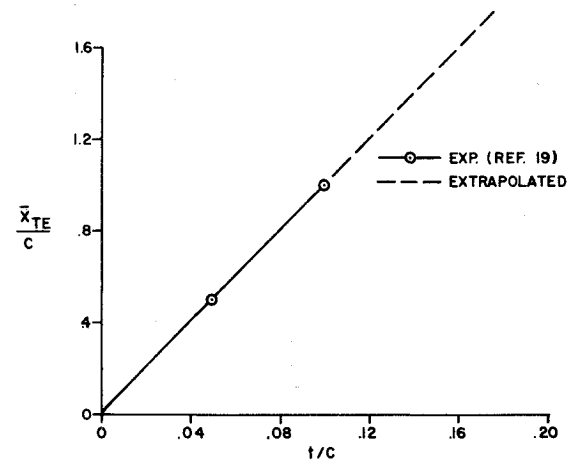

Fig. 9b Distance from base where fins do not affect base pressure. $\bar{X}_{TE}$ = distance from base to tail trailing edge where a fin of given thickness has no affect on base pressure.

Body Base Pressure Drag Increase Due to Presence of Fins

There are several primary factors which determine the effect of fins on base pressure. These factors are fin location, thickness ratio, aspect ratio, profile, sweepback angle, and number of fins. Based on the small amount of experimental data available, it is not possible to accurately account for any of these factors for a general configuration. However, order of magnitude effects of two of the variables, fin location and thickness ratio, can be estimated using Refs. 17-21.

To estimate the effect of fin thickness to chord ratio on base pressure, it will be assumed the fins are flush with the base. The effect of the fins not being flush with the base will be accounted for shortly. Figure 9a is a plot of $\Delta C_{P_B}/(t/c)$ vs Mach number. Here

$$C_{A_B} = \frac{2bC_{P_B}}{S_{\text{ref}}} [(r_{TE})_r + (r_{TE})_t] \tag{15}$$

and $(r_{TE})_t$ are the radius of the trailing-edge bluntness at the root and tip, respectively, the trailing-edge separation drag for cruciform fins can be shown to be

$$\Delta C_{P_B} = (C_{P_B})_{\text{with fins}} - (C_{P_B})_{\text{no fins}}$$

The points above $M_\infty = 1.5$ were taken from the data of Refs. 18 and 19 whereas those points below M_∞ were taken from Ref. 21. Again it should be emphasized that as more data becomes available, this curve could change significantly. For a given Mach number M_1, the increment in base pressure due to the presence of fins is then

$$(\Delta C_{P_B})_f = [(\Delta C_{P_B}/(t/c)]_{M=M_1} (t/c) \tag{16}$$

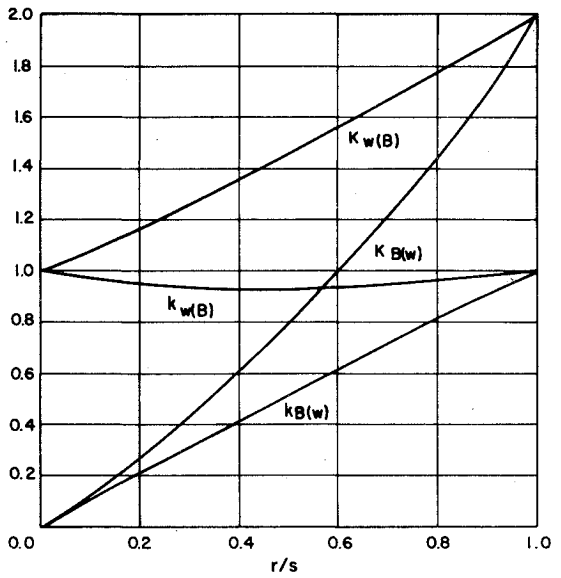

Fig. 10 Slender body interference lift factors.

The values of t/c which Eq. (16) was derived for were 10% or less.

The work of Spahr and Dickey[19] has shown that if the fins were placed upstream a given distance rather than flush with the base, the effect on base pressure is not as great. Furthermore, if the fins were moved far enough from the base, they would have no effect on base pressure; the amount of this movement dependent mainly on fin thickness to chord ratio and profile. As seen in Fig. 9b, this distance varies linearly with t/c up to values of 0.10. The curve in the figure is then extrapolated from $t/c = 0.1$ to $t/c = 0.2$.

Now if a linear variation of $(\Delta C_{P_B})_f$ is assumed between its maximum when the fins are flush with the base and zero when the fins are far enough away from the base, then Eq. (16) may be modified in the form

$$(\Delta C_{P_B})_f = -[(\Delta C_{P_B}/(t/c)]_{m=M_1} [(t/c) - 0.1x/c];$$

$$t/c \geq 0.1x/c$$

$$(\Delta C_{P_B})_f = 0; \quad t/c < 0.1\, x/c \tag{17}$$

x/c in Eq. (17) is the distance (in chord lengths) upstream of the base. This empirical relation was derived only for cruciform fins.

For a given fin thickness to chord ratio and fin location on the body surface, the change in base pressure can be computed and added to the base pressure with no fins. As indicated in Ref. 6, the approximate expression for total base drag is then

$$C_{D_B} = C_{P_B}(d_B/d_{\text{ref}})^3 \tag{18}$$

Wing-Body Interference Lift

Slender body theory as applied by Nielsen et al.[13] is used to compute the interference lift components between the wing and body. Strictly speaking, slender body theory, as indicated in Ref. 13, is for low aspect-ratio wings which do not have sweptback trailing edges. Under these assumptions, the standard interference lift factors are obtained as shown in Fig. 10. Nielsen[13] has shown that good results can be obtained for high aspect-ratio wings even though slender body theory is used. However, for wings with sweptback trailing edges (particularly those of high aspect ratio) the interference lift factors of Fig. 10 must be modified. Figure 11 gives a good indication of how the interference lift factors of Fig. 10 should be changed. Note that for the wing of Fig. 11a for which information is desired, the wing which slender body theory

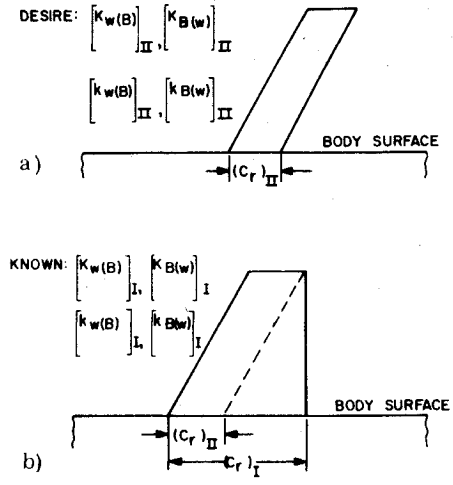

Fig. 11 Procedure used to calculate interference lift for wings with sweptback trailing edges when slender body theory is used: a) wing for which interference lift is desired; b) assumed slender body representation.

assumes is given in Fig. 11b. It is obvious that the interference lift of Fig. 10 is too high. The present approach is to assume that the majority of interference lift is concentrated near the wing root chord and linearly distributed across the chord. Although this appears at first sight to be a rather severe assumption, it tends to give good agreement with experimental data as will be discussed shortly. In equation form, this assumption may be stated as

$$[K_{B(w)}]_{II} = [K_{B(w)}]_{I} G \tag{19a}$$

$$[K_{w(B)}]_{II} = I + ([K_{w(B)}]_{I} - I) G \tag{19b}$$

$$[k_{w(B)}]_{II} = I + ([k_{w(B)}]_{I} - I) G \tag{19c}$$

$$[k_{B(w)}]_{II} = ([k_{w(B)}]_{I} - [k_{w(B)}]_{I}) G \tag{19d}$$

where $G = (c_r)_{II}/(c_r)_{I}$ and the subscript II refers to the actual wing being considered and subscript I refers to the wing for which the slender body interference lift factors of Fig. 10 are valid.

III Comparison with Experiment

The only true test of the validity of assumptions made, as well as the accuracy and usefulness of the general computer program, is to compare it with experimental data. To date, numerous cases have been considered embracing various body and wing geometries, as well as freestream conditions. Many of these cases are presented in Refs. 6, 14, and 22. Since the body alone work has been checked out previously[5,6] emphasis here will be placed on the entire missile or guided projectile configuration.

Three configurations are chosen, the first of these a simple tangent ogive cylinder with tail fins and the remaining two rather complicated configurations. The tangent ogive has a pointed nose and the tail fins have sharp leading and trailing edges with aspect ratio two. Figure 12a compares the theoretical drag, normal force coefficient derivative, and center of pressure as a function of Mach number with experimental data. Figure 12b compares the same coefficients as a function of angle of attack for Mach 1.3. The experimental data are taken from Ref. 23. The agreement here is within ±10% on force coefficients and center of pressure within a half caliber.

A more complicated wing-body configuration is considered in Figs. 13a and 13b. This case has a 40% blunt nose with a boattail present. The tail fins are aspect ratio 4.5 with a modified double wedge airfoil section. The airfoil section has

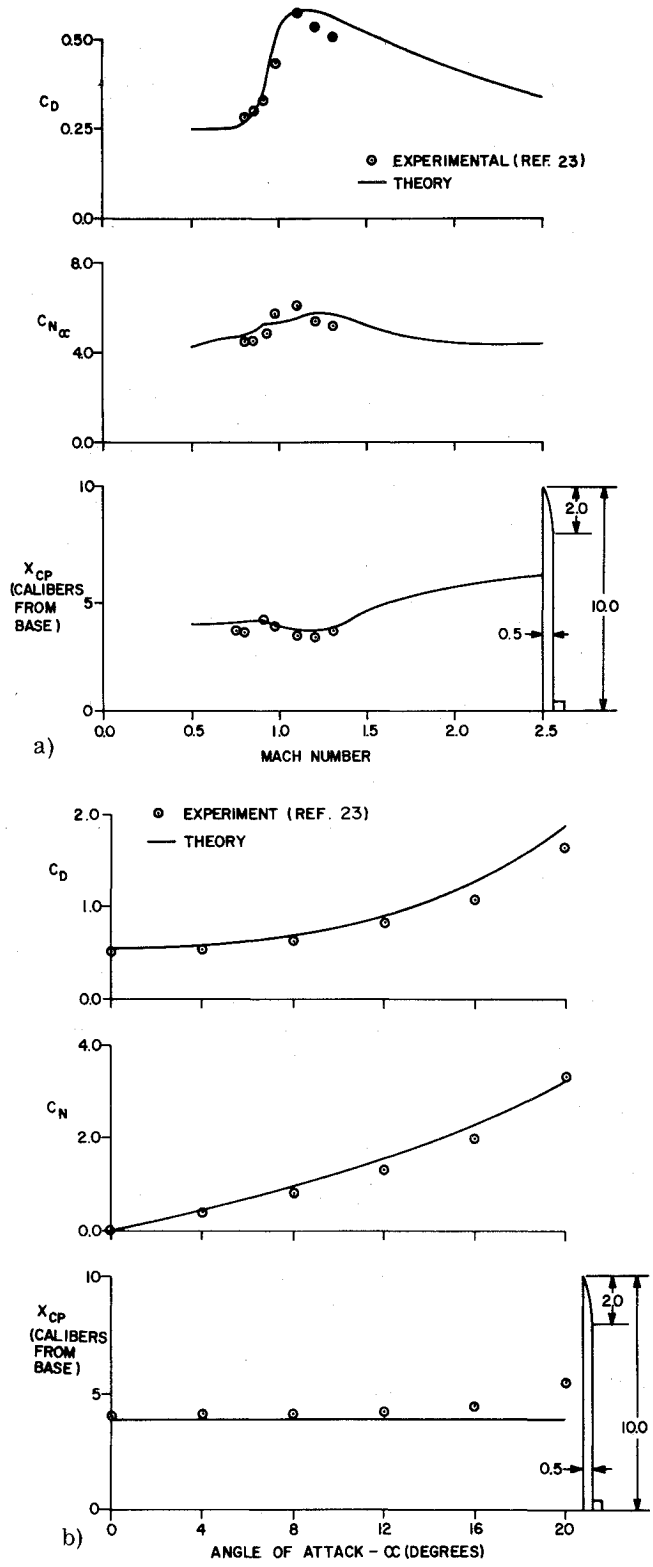

Fig. 12 Static aerodynamics of a missile configuration: a) $\mathcal{R} = 2.0$, $\Lambda = 0°$, $\lambda = 1.0$, and $\alpha = 1°$; b) $\mathcal{R} = 2.0$, $\Lambda = 0°$, $\lambda = 1.0$, and $M_\infty = 1.3$.

blunt leading and trailing edges (similar to Fig. 7). Referring to Figs. 13a and 13b, the theoretical drag is high in the transonic range by about 10% but otherwise the agreement on all force coefficients is good. The agreement of theory and experiment on normal force coefficient at transonic Mach numbers is better than expected considering the empirical nature of the methods used in that Mach number regime. On the other hand, the empirical method can only be as good as the theoretical values of C_N at $M_\infty = 1.2$ and $M_\infty = 0.85$ (which is the force break Mach number).

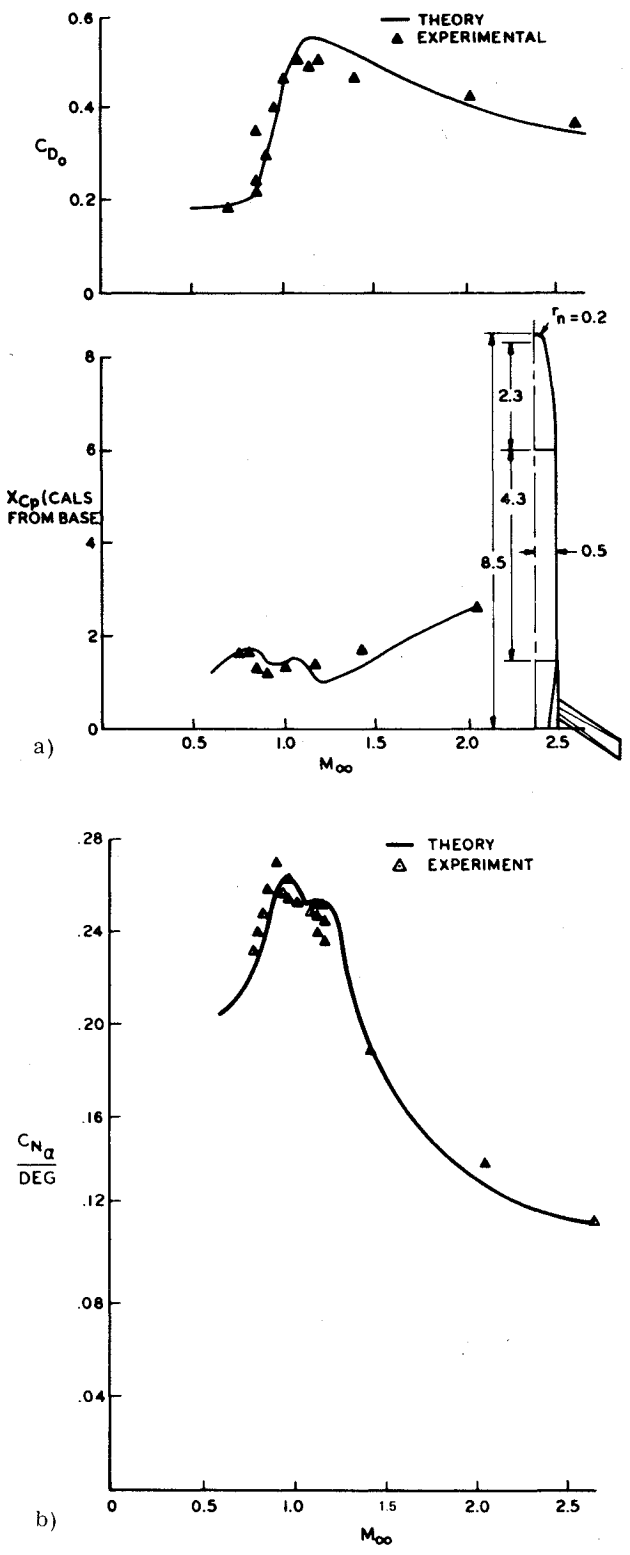

Fig. 13 Missile configuration, $\mathcal{R}=4.5$; a) drag and center of pressure; b) normal force coefficient derivative.

The final example chosen is a complex canard-body-tail configuration. The body nose is 60% blunt with two ogive segments and a 0.7 caliber boattail. The canard has an aspect ratio of two with a sweepback angle of 15°. Its shape consists of a sharp wedge leading edge with a constant thickness section following. The trailing edge is truncated parallel to the leading edge. The tail has an aspect ratio of four with cylindrical leading and trailing edges and where $\Lambda_1 = 30°$, $\Lambda_2 = 2.25°$, $\Lambda_3 = 37°$, and $\Lambda_4 = 30°$. The tail thickness to chord ratio also varies along the span. The detailed canard and wing geometry previously listed is not needed in calculating lift, but it must be known for drag computations. The results of the calculations for this configuration are shown in Fig. 14. Figure 14a gives the normal force and center of pressure for $M_\infty = 1.6$ and at various angles of attack. Four curves are shown in the figure: canard-body-tail with canards deflected by 10°, canard-body-tail with no canard deflection, body-tail, and finally body alone. Several points are worthy of note in this figure. First of all the body-alone solution agrees very well with the unpublished experimental data up to $\alpha = 16°$. Above $\alpha = 16°$, the theory is low which is probably due to not taking into account Reynolds's number effect in the body crossflow drag coefficient. The next point is that for this configuration, the tail lift is about 10% too high and the canard lift about 15% too low so that the total lift agrees almost perfectly with the experimental data up to the point where stall begins to occur ($\alpha \geq 14°$). This in turn causes the center of pressure to be more rearward than the experimental data suggest by about half a caliber. It is suspected that the theory being high for the high aspect-ratio tail and low for the moderate aspect-ratio canard is due to the flowfield interaction effects from the complex configuration and will not in general be true for other cases. However, it does indicate that the theory can be used quite effectively in design, even for quite complex wing-body-tail geometries. The final point to be emphasized from Fig. 14a is the fact that no attempt has been made to predict stall characteristics. As seen in the figure, for this configuration, stall occurs around $\alpha = 15°$ at $M_\infty = 1.6$. However, if the wing thickness or freestream Mach number is changed the stalling angle of attack will also change.

The drag characteristics for this same missile are shown in Fig. 14b. The drag is shown as a function of Mach number and again the total force is broken down into its components: body alone, body tail, and canard-body-tail. The body-alone drag is acceptable in supersonic and subsonic flow but is unacceptable in transonic flow where the empirical nature of the theory does not account for nose bluntness. The wing-alone drag shown at the bottom figure, includes the increase in base drag due to tails. This causes the tail drag to be high because the theory predicts this base drag increase to be significantly higher than the experimental data suggest. However, the body-tail drag is still within the ±10% category. Finally, the canard drag shown at the bottom figure, is added to the body-tail drag and the overprediction of tail drag is compensated somewhat by the underprediction of canard drag.

As was mentioned earlier, the tail has a cylindrical leading edge for which the combined Newtonian perturbation theory must be used to calculate the pressure coefficient. Figure 14c presents this pressure coefficient in the vicinity of the leading edge for Mach 2 and at a spanwise station of $y/(b/2) = 12.5\%$. The discontinuity in pressure coefficient caused by the difference in Newtonian and perturbation theory estimates occurs at a match point of $x/c \cong 0.009$.

IV. Computational Time and Cost

Although the method presented herein for computing aerodynamics of guided or unguided projectiles actually consists of several rather complicated theoretical and empirical procedures, the cost to obtain force and moment predictions is relatively small. For example, the most complicated configuration considered to date was the canard-body-tail shape in Fig. 14. To compute the aerodynamics at ten Mach numbers for a small angle-of-attack takes about 5 min on the CDC 6700 Computer or costs about $75. Aerodynamics at supersonic Mach numbers costs about twice as much per Mach number than at subsonic or transonic Mach numbers. If the body has a pointed nose, or if there are no canards, or if the tails are absent, this time and cost can be reduced considerably. For example, consider the pointed body-tail configuration of Fig. 12. This case took less than two minutes of execution time for ten Mach numbers and cost about $25. It is

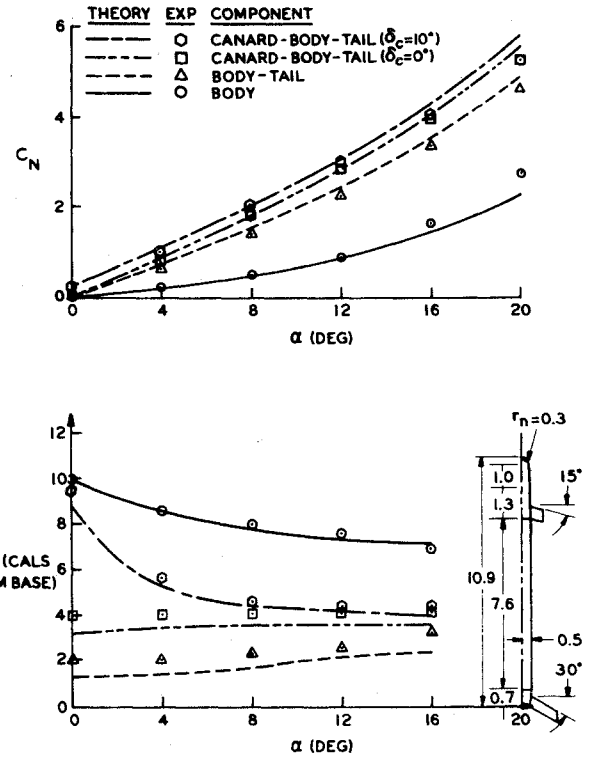

Fig. 14a Normal force and center of pressure of a missile configuration; $\mathcal{R}_t = 4$, $\mathcal{R}_c = 2$, and $M_\infty = 1.6$.

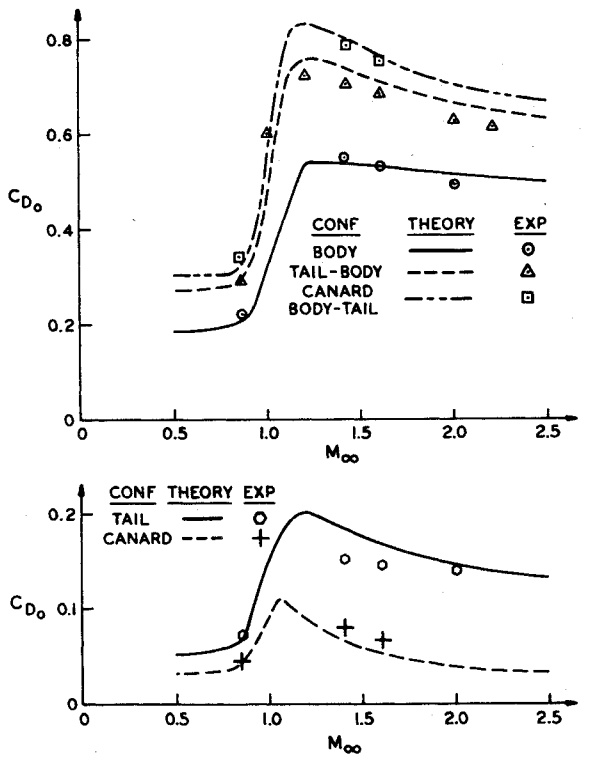

Fig. 14b Drag of a missile configuration and its components.

thus believed that the present method is very cost effective compared to experimental methods in that reasonably accurate results for forces and moments can be obtained at a very small cost.

V. Conclusions and Recommendations

1) A general method has been developed consisting of several theoretical and empirical procedures to calculate lift, drag, and center of pressure on wing-body-tail configurations from Mach 0 to about 3 and for angles of attack to about 15°.

2) Comparison of this method with experiment for several configurations indicates that accuracies of ±10% can be obtained for force coefficients of most configurations. This is at a cost of $75 or less for ten Mach numbers in the range $0 \leq M_\infty \leq 3$.

3) Second-order perturbation theory can be combined with modified Newtonian theory to adequately predict pressures on general shaped bodies of revolution. This is true for supersonic Mach numbers as pow as 1.2 even though Newtonian theory was derived for high Mach-number flow. First-order perturbation theory can be used in conjunction with modified Newtonian theory, to calculate wave drag on wings with blunt leading edges. However, at low supersonic Mach numbers ($M_\infty < 1.5$) relatively large discontinuities in pressure coefficient exist at the match point.

4) Wave drag of wings with variable airfoil section and thickness to chord ratio along the span can still be calculated by conical flow theory if the local source strength is computed at each point on the wing and based on the local slope at the point.

5) Changes in body base pressure due to the presence of tail surfaces is not known sufficiently for all airfoil shapes. It is recommended that a systematic wind tunnel study be conducted for Mach number, $0 \leq M_\infty \leq 3$, angle of attack, $0 \leq \alpha \leq 20°$, and various airfoil geometries to empirically estimate this change.

6) Although much progress has been made in transonic flow theory, no simple method exists for calculating wing lift or wave drag on complicated wing configurations. It is thus recommended that much work continue in this area until practical tools are developed.

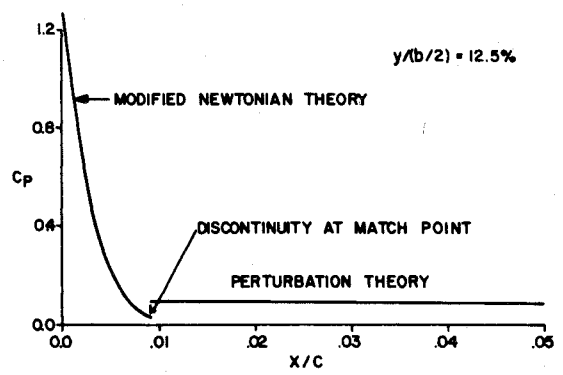

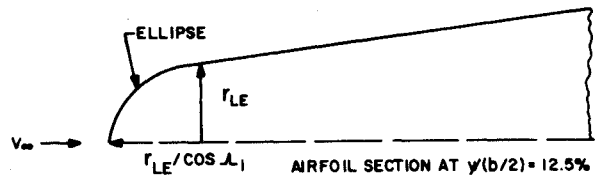

Fig. 14c Pressure coefficient on leading edge of a blunt leading-edge wing; $\Lambda_1 = 30°$, $M_\infty = 2$, $b = 0.92'$, $C_r = 0.23'$, $r_{LE} = 0.0021'$, $t_r = 0.0167'$, and $t_t = 0.0042'$.

References

[1]Douglas Aircraft Co., Inc., *USAF Stability and Control DATCOM,* July 1963, 2 Vols., Revisions by the U.S. Air Force, Wright-Patterson Air Force Base, Ohio.

[2]Woodward, F.A., "Analysis and Design of Wing-Body Combinations at Subsonic and Supersonic Speeds," *Journal of Aircraft,* Vol. 5, June 1968, pp. 528-534.

[3]Saffell, B.F., Jr., Howard, M.L., and Brooks, E.N., Jr., "A Method for Predicting the Static Aerodynamic Characteristics of Typical Missile Configurations for Angles-of-Attack to 180 Degrees," NSRDC Rept. 3645, 1971.

[4]Whyte, R.H., "Spinner—A Computer Program for Predicting the Aerodynamic Coefficients of Spin Stabilized Projectiles," General Electric Class 2 Reports, 1969, General Electric Co., Philadelphia, Pa.

[5]Moore, F.G., "Aerodynamic Drag and Lift of General Body Shapes at Subsonic, Transonic, and Supersonic Mach Numbers," AGARD Conference Preprint No. 124 on Aerodynamic Drag, Paper No. 2, 1973, Izmir, Turkey.

[6]Moore, F.G., "Body Alone Aerodynamics of Guided and Unguided Projectiles at Subsonic, Transonic, and Supersonic Mach Numbers," NWL TR-2796, 1972, Naval Weapons Lab., Dahlgren, Va.

[7]Van Dyke, M.D., "A Study of Second-Order Supersonic Flow Theory," Rept. 1081, 1952, NACA.

[8]Van Dyke, M.D., "Practical Calculation of Second-Order Supersonic Flow Past Nonlifting Bodies of Revolution," TN-2744, July 1952, NACA.

[9]Van Dyke, M.D, "First-and Second-Order Theory of Supersonic Flow Past Bodies of Revolution," *Journal of the Astronautical Sciences,* Vol. 18, March 1951, pp. 161-179.

[10]Jackson, C.M., Jr., Sawyer, W.C., and Smith, R.S., "A Method for Determining Surface Pressures on Blunt Bodies of Revolution at Small Angles-of-Attack in Supersonic Flow," TN D-4865, 1968, NASA.

[11]Jones, R.T. and Cohen, D., *High Speed Wing Theory,* Princeton Aeronautical Paperbacks, No. 6, 1960.

[12]Chadwick, W.R., "The Application of Non-Planar Lifting Surface Theory to the Cclculation of External Store Loads," *AIAA Journal,* Vol. 11, March 1974, pp. 181-188.

[13]Pitts, W.C., Nielsen, J.N., and Kaattari, G.E., "Lift and Center of Pressure of Wing-Body-Tail Combinations at Subsonic, Transonic, and Supersonic Speeds," TR 1307, 1957, NACA.

[14]Van Driest, E.R., "Turbulent Boundary Layer in Compressible Fluids," *Journal of the Astronautical Sciences,* Vol. 18, 1951, pp. 145-160, 216.

[15]Moore, F.G., "Aerodynamics of Guided and Unguided Weapons: Part I—Theory and Application," NWL TR-3018, Dec. 1973, Naval Weapons Lab., Dahlgren, Va.

[16]Ferri, Antonio, *Elements of Aerodynamics of Supersonic Flows,* Macmillan, New York, 1949, pp. 292-343.

[17]Chapman, D.R., Wimbrow, W.R., and Kester, R.H., "Experimental Investigation of Base Pressure on Blunt-Trailing-Edge Wings at Supersonic Velocities," Rept. 1109, 1952, NACA (Supercedes NACA TN-2611).

[18]Heyser, A., Maurer, F., and Oberdorffer, E., "Experimental Investigation on the Effect of Tail Surfaces and Angle-of-Attack on Base Pressure in Supersonic Flow," *Proceedings, The Fluid Dynamic Aspects of Ballistics,* AGARD-CP-10, 1966, pp. 263-290.

[19]Spahr, J.R. and Dickey, R.R., "Effect of Tail Surfaces on the Base Drag of Body of Revolution at Mach Numbers of 1.5 and 2.0," TN-2360, 1951, NACA.

[20]Love, E.S., "Base Pressure at Supersonic Speeds on Two-Dimensional Airfoils and on Bodies of Revolution With and Without Turbulent Boundary Layers," TN-3819, 1957, NACA.

[21]Krens, F.J., "Full-Scale Transonic Wind Tunenl Test of the 8-Inch Guided Projectile," NWL TR-2535, 1971, Naval Weapons Lab., Dahlgren, Va.

[22]Moore, F.G., and McKerley, C.W., "Aerodynamics of Guided and Unguided Weapons; Part II—Computer Program and Usage," NWL TR-3036, 1974, Naval Weapons Lab., Dahlgren, Va.

[23]Craft, J.C. and Skorupski, J., "Static Aerodynamic Stability Characteristics of Munitions Designs at Transonic Mach Numbers," Rept. RD73-3, U.S. Army Missile Command, Redstone Arsenal, Alabama.